JCB Report

# Impaired membrane resealing and autoimmune myositis in synaptotagmin VII–deficient mice

**Sabyasachi Chakrabarti,[1] Koichi S. Kobayashi,[2] Richard A. Flavell,[2] Carolyn B. Marks,[3,4] Katsuya Miyake,[6] David R. Liston,[1,3] Kimberly T. Fowler,[1,3] Fred S. Gorelick,[3,5] and Norma W. Andrews[1,3]**

[1]Section of Microbial Pathogenesis, Boyer Center for Molecular Medicine, [2]Section of Immunobiology, Howard Hughes Medical Institute, [3]Department of Cell Biology, [4]Center for Cell and Molecular Imaging, [5]Section of Digestive Diseases, Department of Internal Medicine, Yale University School of Medicine, New Haven, CT 06510
[6]Institute of Molecular Medicine and Genetics, Medical College of Georgia, Augusta, GA 30912

Members of the synaptotagmin family have been proposed to function as $Ca^{2+}$ sensors in membrane fusion. Syt VII is a ubiquitously expressed synaptotagmin previously implicated in plasma membrane repair and *Trypanosoma cruzi* invasion, events which are mediated by the $Ca^{2+}$-regulated exocytosis of lysosomes. Here, we show that embryonic fibroblasts from Syt VII–deficient mice are less susceptible to trypanosome invasion, and defective in lysosomal exocytosis and resealing after wounding. Examination of mutant mouse tissues revealed extensive fibrosis in the skin and skeletal muscle. Inflammatory myopathy, with muscle fiber invasion by leukocytes and endomysial collagen deposition, was associated with elevated creatine kinase release and progressive muscle weakness. Interestingly, similar to what is observed in human polymyositis/dermatomyositis, the mice developed a strong antinuclear antibody response, characteristic of autoimmune disorders. Thus, defective plasma membrane repair in tissues under mechanical stress may favor the development of inflammatory autoimmune disease.

## Introduction

Synaptotagmins are transmembrane proteins with a short lumenal domain and two functional $Ca^{2+}$-binding domains ($C_2A$ and $C_2B$) in their cytosolic region. The brain-specific isoform Syt I resides on synaptic vesicles, where it plays a critical role in rapid $Ca^{2+}$-triggered neurotransmitter release, through interactions mediated by its $C_2A$ and $C_2B$ domains (Chapman, 2002). Although several of the additional isoforms also appear to be primarily expressed in the brain, ubiquitously expressed synaptotagmins have been identified (Li et al., 1995; Craxton and Goedert, 1999). Syt VII, in particular, is widely expressed in neuronal and nonneuronal tissues in a relatively uniform manner (Ullrich and Sudhof, 1995), which is consistent with its localization on conventional lysosomes (Martinez et al., 2000; Caler et al., 2001).

$Ca^{2+}$-regulated exocytosis of lysosomes was recently recognized as a ubiquitous process, which is not restricted to specialized secretory cells. Several cell types, such as fibroblasts and epithelial cells, respond to $Ca^{2+}$ elevations by exposing lysosomal proteins on the plasma membrane and by releasing lysosomal contents (Rodriguez et al., 1997). Among several fluorescently tagged intracellular compartments analyzed by total internal reflection fluorescence microscopy, membrane-proximal lysosomes were found to be the major $Ca^{2+}$-regulated exocytotic population (Jaiswal et al., 2002). In addition to other markers, these membrane-proximal lysosomes also contain Syt VII (Jaiswal et al., 2002). These findings are consistent with previous studies implicating Syt VII in the regulation of lysosomal exocytosis (Martinez et al., 2000), in the lysosome-mediated cell invasion mechanism of *Trypanosoma cruzi* (Caler et al., 2001), and in the process by which cells repair plasma membrane wounds (Reddy et al., 2001).

$Ca^{2+}$ influx at the site of membrane injury triggers exocytosis, a process thought to be essential for cell resealing (McNeil and Steinhardt, 1997). Lysosomes are likely candidates for the vesicular population involved in this process, because inhibition of lysosomal exocytosis by introducing recombinant Syt VII $C_2A$, anti-Syt VII $C_2A$, or anti–Lamp-1 antibodies greatly reduced the efficiency of plasma membrane resealing in wounded fibroblasts (Reddy et al., 2001). Thus, a major

Address correspondence to Norma W. Andrews, Section of Microbial Pathogenesis, Boyer Center for Molecular Medicine, Yale University School of Medicine, 295 Congress Ave., New Haven, CT 06510. Tel.: (203) 737-2410. Fax: (203) 737-2630. email: norma.andrews@yale.edu

Key words: exocytosis; repair; lysosome; inflammatory myopathy; knockout mouse

Abbreviations used in this paper: DMEM, Dulbecco's minimal essential medium; ES, embryonic stem; LDH, lactate dehydrogenase; MEF, murine embryonic fibroblast.

role of $Ca^{2+}$-triggered lysosomal exocytosis might be the maintenance of plasma membrane integrity. However, very limited information is available on the physiological consequences of defective membrane repair. A role for the sarcolemma protein dysferlin in a muscle-specific resealing mechanism was recently suggested, although the nature of the putative exocytotic vesicles involved in that process is still unknown (Bansal et al., 2003). To investigate the in vivo consequences of disrupting $Ca^{2+}$-dependent exocytosis mediated by the ubiquitously expressed Syt VII, we performed targeted gene disruption in mice by homologous recombination.

## Results and discussion

A targeting vector was constructed to replace the first $Ca^{2+}$-binding $C_2A$ domain of the *Syt VII* gene with the neomycin (*neo*$^R$) cassette (Fig. 1 A). Embryonic stem (ES) cells were electroporated with the targeting vector and two independently derived, correctly targeted ES cell clones (Fig. 1 B) were microinjected into C57BL/6 blastocysts. Chimeric mice were bred to female C57BL/6 mice, and successful germinal transmission of the mutated allele was monitored by Southern blot analysis of genomic DNA from the offspring. Heterozygous mice were interbred to produce offspring homozygous for the *Syt VII* deletion (Fig. 1 C). Syt VII–deficient mice were born at the expected Mendelian ratio, showing no gross abnormalities and no obvious neurological defects. The mutant mice appear to have a normal life span and are fertile, although their reproductive capacity seems to decline faster with age (the average litter size from 20 breeding pairs older than 6 mo was 7 ± 2 in wild-type, and 3 ± 2 in Syt VII $^{-/-}$ mutants).

Absence of the 1.2-kb mRNA corresponding to the major Syt VII α isoform (Fukuda et al., 2002) was verified by Northern blot analysis (Fig. 1 D). Western blots showed that disruption of the *Syt VII* gene abolished expression of the full-length <66-kD protein (Fig. 1 E). Because the region containing the $C_2$ domains is highly conserved among synaptotagmin isoforms (Li et al., 1995), the anti-Syt VII antibodies were generated against a recombinant peptide comprising amino acids 46–133 of the unique Syt VII spacer domain (Sugita et al., 2001). The targeting vector generated a stop codon after the position coding for amino acid 83 in exon 4, thus, making it possible that the low $M_r$ band recognized by the antibodies in Syt VII −/− extracts (Fig. 1 E, bottom) corresponds to a short mutated protein comprising the lumenal domain, the transmembrane region, and only a fraction of the spacer domain. This is consistent with the results of RT-PCR analysis of RNA from mouse tissues (Fig. 1 F). A 210-bp fragment corresponding to the

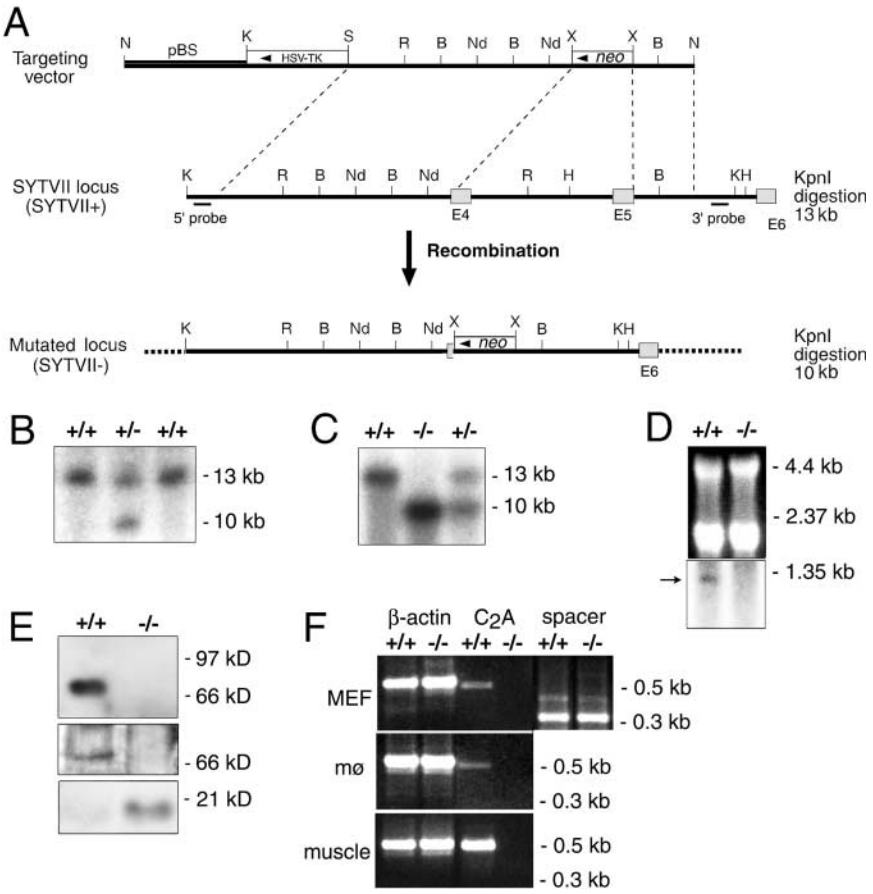


Figure 1. **Generation of Syt VII −/− mice by gene targeting.** (A) Schematic representation of the Syt VII genomic locus, the targeting vector, and the targeted locus. Exons 4–6 are shown as boxes. Restriction enzyme sites (N, NotI; K, KpnI; S, SalI; R, EcoRI; B, BamHI; Nd, NdeI; X, XhoI; H, HindIII) and the 5′ and 3′ external probes are indicated. (B) Southern blot analysis of ES cells showing one of the injected clones (+/−) and two wild-type clones (+/+). (C) Southern blot analysis of tail DNA derived from Syt VII wild-type (+/+), homozygous (−/−), and heterozygous (+/−) animals analyzed with 5′ and 3′ external probes. The sizes of the wild-type and mutant alleles are indicated. (D) Northern blot analysis of RNA from wild-type (+/+) and homozygous (−/−) MEFs (bottom). The concentration of the RNA samples was assessed by ethidium bromide staining of the 28S and 18S RNA (top). (E) Immunoblot analysis of extracts prepared from wild-type (+/+) and homozygous (−/−) bone marrow macrophages (top) and quadriceps muscle (bottom) probed with affinity-purified antibodies against the Syt VII membrane proximal domain. (F) RT-PCR analysis of cDNA from MEFs, bone marrow macrophages (mø), and quadriceps muscle from wild-type (+/+) and Syt VII–deficient (−/−) mice, using primers directed to the $C_2A$ (forward, 5′-CCAGACGCCACACGATGAGTC-3′; and reverse, 5′-CCTTCCAGAAGGTCTGCATCTGG-3′) or membrane proximal spacer (forward, 5′-CCCGCGATGTCCTGCTGGTCT-3′; and reverse, 5′-GTATTCACAGCCTTCCCTCCTGC-3′) domains of Syt VII. Amplification of β-actin cDNA was included as a control.

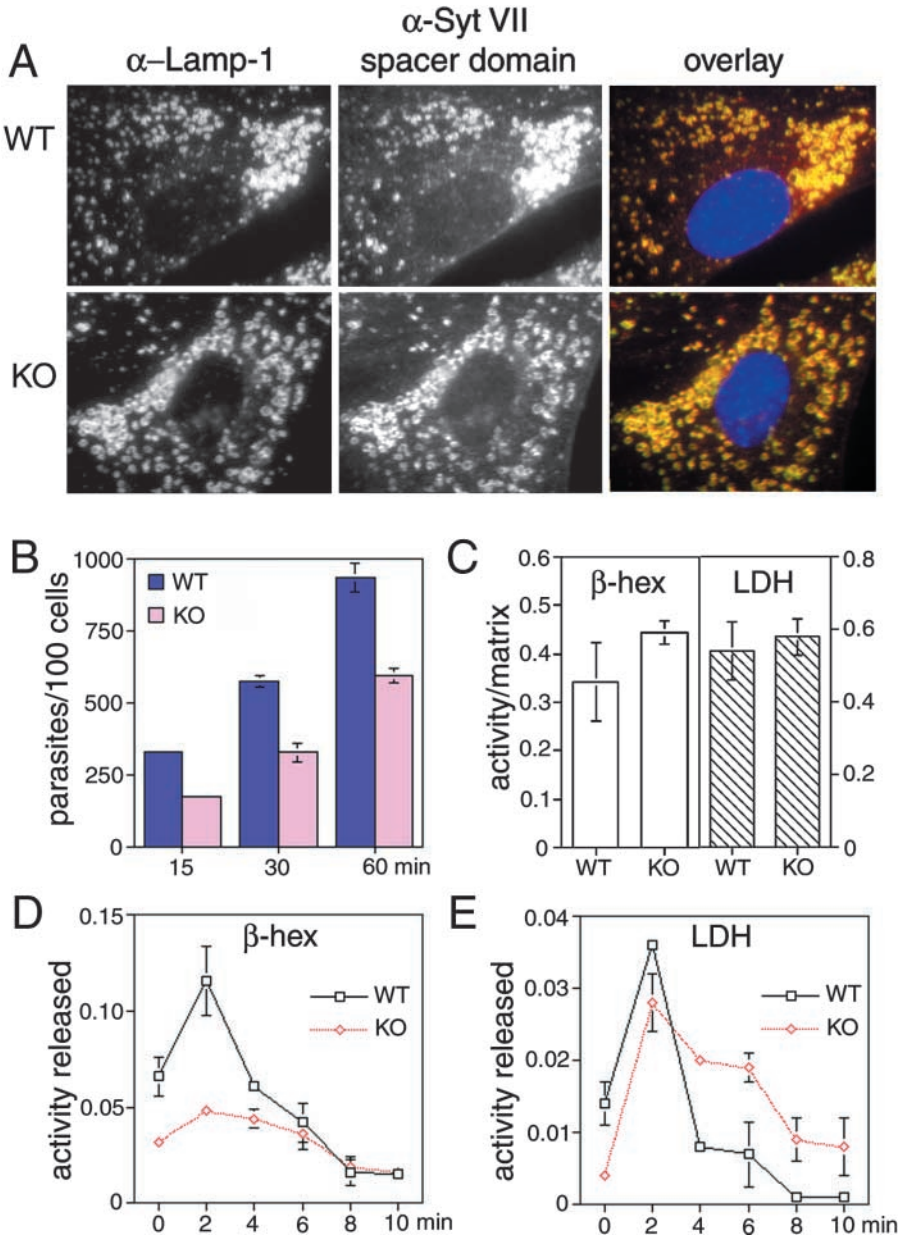


Figure 2. **Decreased susceptibility to *T. cruzi* invasion and defective lysosome-mediated membrane repair.** (A) Immunofluorescence of wild-type (WT) and Syt VII–deficient (KO) MEFs with antibodies to Lamp-1 and to the spacer domain of Syt VII, indicating that both wild-type and mutated forms of Syt VII are targeted normally to lysosomes. Yellow reflects regions of overlay between anti–Lamp-1 (green) and anti–Syt VII spacer domain (red). (B) Invasion of WT and KO MEFs by *T. cruzi*. MEFs were exposed to trypomastigotes for the indicated periods of time, washed, and processed for detection of intracellular parasites using an inside/outside immunofluorescence assay. The data represent the average of triplicates ± SD. (C) Total β-hexosaminidase and LDH activity in fibroblast-collagen matrices prepared from WT or KO mice. Enzymatic activity was assayed in detergent extracts. The data represent the average of triplicate matrices ± SD. (D) Release of lysosomal β-hexosaminidase during contraction and wounding of WT or KO MEF-collagen matrices. Matrices were released from the dish at t = 0 and the supernatant was removed and replaced at 2-min intervals for determination of β-hexosaminidase activity. The data represent the average of triplicate matrices ± SD. (E) Release of cytosolic LDH during contraction and wounding of WT or KO MEF-collagen matrices. Matrices were released from the dish at t = 0 and the supernatant was removed and replaced at 2-min intervals, for determination of LDH activity. The data represent the average of triplicate matrices ± SD.

region encoding amino acids 1–83 of the major Syt VII α isoform (Fukuda et al., 2002) was amplified from cells of both wild-type and mutant mice (Fig. 1 F, top). A faint 340-bp band was also detected, in agreement with the predicted size for the minor alternatively spliced Syt VII β isoform (Fukuda et al., 2002). In contrast, a 504-bp fragment corresponding to the $C_2A$ domain was amplified from several cell types derived from wild-type, but not Syt VII–deficient mice (Fig. 1 F). Thus, consistent with our gene targeting strategy, disruption of the *Syt VII* gene abolished expression of both $C_2$ domains, the critical functional regions responsible for the calcium-dependent interactions previously detected in synaptotagmins (Chapman, 2002; Yoshihara and Littleton, 2002).

The $NH_2$-terminal, membrane-proximal region of synaptotagmins has been reported to mediate $Ca^{2+}$-independent clustering (Bai et al., 2000; Fukuda et al., 2001a), so a putative dominant negative effect mediated by this domain cannot be ruled out. Immunofluorescence results with antibodies against the membrane-proximal Syt VII spacer domain, however, show that both the wild-type and mutated forms of Syt VII are detected in a normal lysosomal localization pattern, with no evidence of aggregation or mistargeting (Fig. 2 A). Therefore, as previously reported for the Golgi-targeted synaptotagmin isoform Syt IV (Fukuda et al., 2001b), our results indicate that the targeting signal of Syt VII is located within the membrane proximal spacer region (unpublished data).

Murine embryonic fibroblasts (MEFs) derived from Syt VII–deficient mice were less susceptible to invasion by the protozoan parasite *T. cruzi* (Fig. 2 B), which is consistent with what was previously reported for CHO cells transfected with the inhibitory Syt VII $C_2A$ domain (Caler et al., 2001). Because this parasite uses $Ca^{2+}$-regulated lysosomal exocytosis for invasion (Tardieux et al., 1992), the fact that the overall number and morphology of lysosomes was not altered in

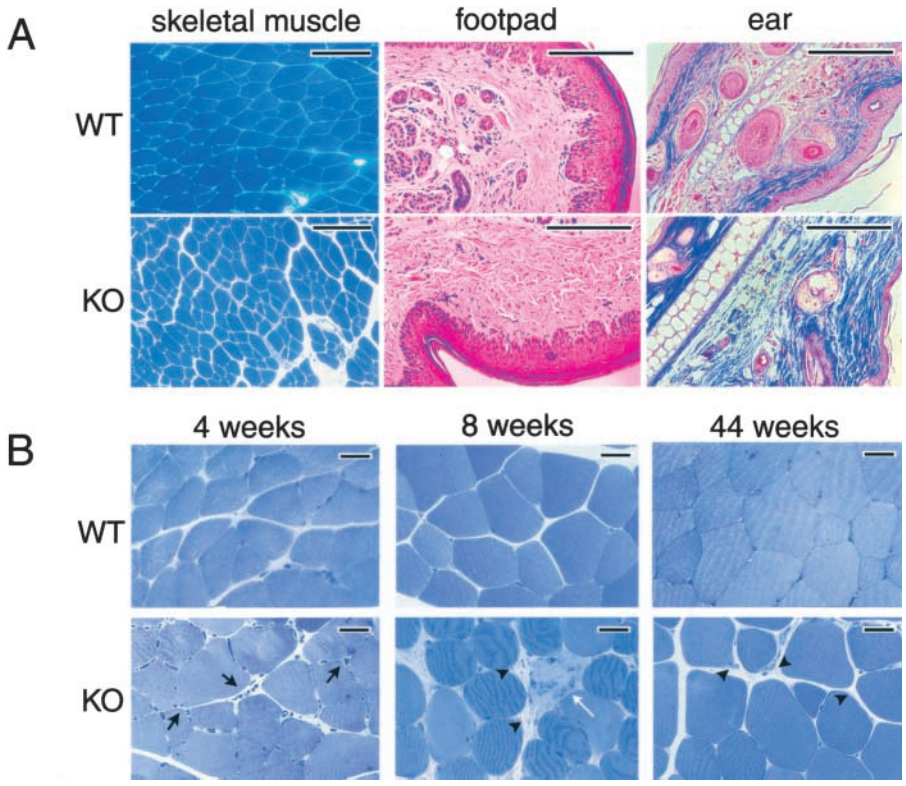


Figure 3. **Inflammation, injury, and fibrosis in skin and skeletal muscle.** (A) Histological sections of quadriceps muscle, footpad, and ear of 14-wk-old male wild-type (WT) and Syt VII–deficient (KO) mice. Increased accumulation of connective tissue is evident in the sections of KO mice. Skeletal muscle sections are stained with toluidine blue, footpad sections with H&E, and skin sections with Masson's trichrome, which stains collagen fibers in blue. Bars, 100 μm. (B) Toluidine blue–stained sections of quadriceps muscle from male WT and KO mice at 4, 8, and 44 wk old. Infiltration of inflammatory cells is initially detected (black arrows), followed by tissue injury, fiber invasion by phagocytic cells (white arrow), and collagen deposition (black arrowheads). Bars, 25 μm.

Syt VII–deficient MEFs (Fig. 2 A) suggested that the defect might reside in the $Ca^{2+}$-triggered membrane fusion step. Therefore, we next investigated the ability of wild-type and Syt VII–deficient MEFs to undergo lysosomal exocytosis in a physiological model of membrane wounding and repair. Previous studies showed that fibroblasts embedded in collagen matrices undergo contraction and plasma membrane wounding when the matrix is released from the substrate, a process followed by rapid resealing (Lin et al., 1997). When matrices are lifted in the presence of inhibitory soluble Syt VII $C_2A$ domain or of antibodies against this domain, the exocytosis of lysosomes that occurs simultaneously with wounding is inhibited, and fibroblasts fail to reseal (Reddy et al., 2001). A similar pattern was observed in MEFs from Syt VII–deficient mice. Wild-type and mutant MEF extracts contained comparable amounts of lysosomal β-hexosaminidase and cytosolic lactate dehydrogenase (LDH; Fig. 2 C), but significantly less β-hexosaminidase was released when Syt VII −/− MEF matrices were lifted to induce contraction and wounding (Fig. 2 D). In contrast, leakage of cytosolic LDH from wounded Syt VII −/− cells remained elevated for a significantly longer period, when compared with matrices containing wild-type MEFs (Fig. 2 E). This pattern, observed in several independent experiments, indicates that a major consequence of defective lysosomal exocytosis in wounded Syt VII −/− cells is an alteration in the kinetics of the repair process.

To investigate the consequences of impaired resealing in the mouse tissues, histological examination of various organs was performed in 14-wk-old wild-type and Syt VII–deficient littermates. No obvious abnormalities were detected in the brain, liver, heart, exocrine pancreas, spleen, or kidneys of the mutant mice (unpublished data). However, sections of the skin and skeletal muscle showed an enhanced accumulation of connective tissue elements, indicative of fibrosis (Fig. 3 A). Examination of the skeletal muscle of younger animals revealed an extensive endomysial cellular infiltration in 4-wk-old mutant mice, and scattered foci of inflammation and fiber degeneration at 8 wk old (Fig. 3 B, left and center). At this stage, several muscle fibers were completely surrounded by inflammatory cells, and invasion of degenerating fibers by macrophages and eosinophils was apparent on light (Fig. 3 B, center) and electron microscopy analysis (Fig. 4 A). Mast cells and bundles of collagen fibers were frequently observed in the endomysial space (Fig. 4 A). The presence of inflammatory cells infiltrating the skeletal muscle of 8-wk-old Syt VII −/− mice was confirmed by immunocytochemistry with specific antibodies against markers of T cells (CD3), macrophages and NK cells (CD11b), and neutrophils and eosinophils (Ly-6G) (Fig. 4 B). Inflammatory cells were less abundant in the skeletal muscle of older Syt VII −/− mice but fibrosis remained detectable until 44 wk old (Fig. 3 B; Fig. 5 A).

Further analysis was performed to verify if Syt VII–deficient mice had features considered diagnostic of inflammatory myopathies, as suggested by the histological examination. Accumulation of collagen in the skin and skeletal muscle was confirmed through biochemical assays of total tissue hydroxyproline content (Hao et al., 2000). An apparently life-long elevation in collagen deposition was observed in skin and skeletal muscle but not in the liver (Fig. 5 A), heart, spleen, and kidneys (not depicted). Syt VII mutant mice also had elevated levels of serum creatine kinase, which is an important diagnostic marker for muscle fiber injury (Bogdanovich et al., 2002; Fig. 5 B). Decreased forelimb grip strength (LaMonte et al., 2002) was detected in mutant

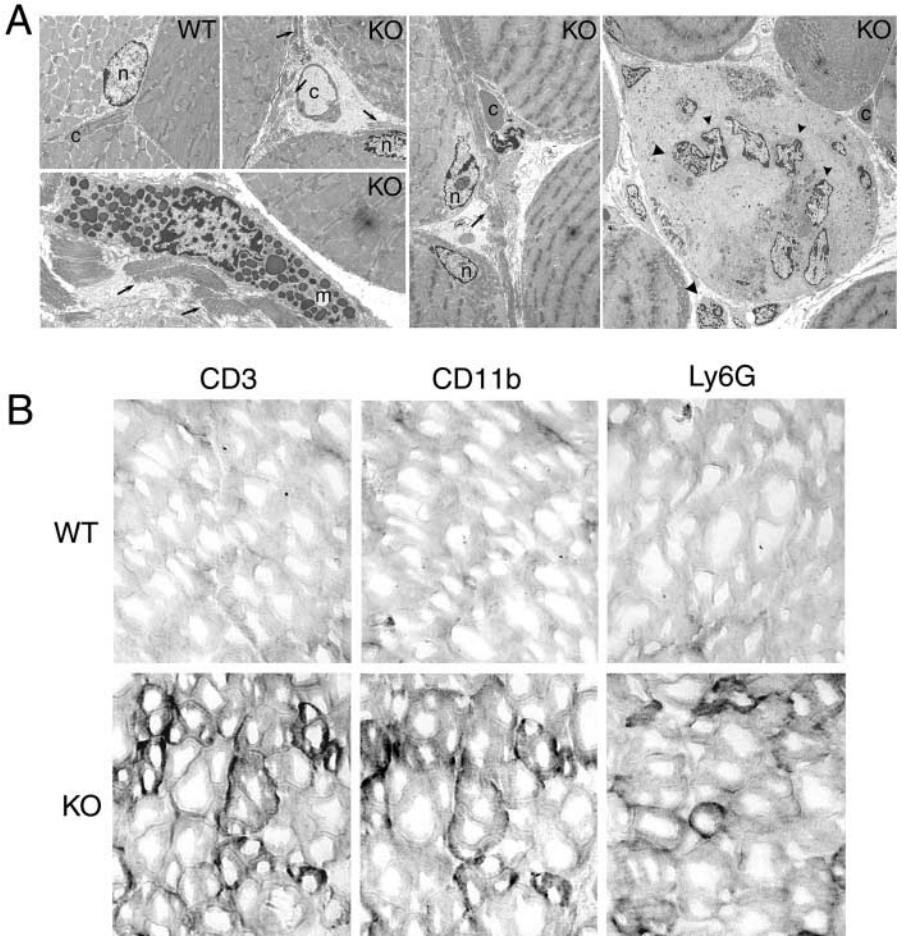


Figure 4. **Inflammatory cells in skeletal muscle.** (A) Electron micrographs of sections from the quadriceps muscle of 8-wk-old male wild-type (WT) and Syt VII–deficient (KO) mice. In contrast to WT muscle (top left), in mutant animals, the collagen accumulation and infiltration of inflammatory cells is evident. Arrows point to bundles of collagen fibers, large arrowheads to eosinophils, and small arrowheads to macrophages; n indicates muscle fiber nuclei; c, capillaries; and m, mast cell. (B) Detection of inflammatory cells in the skeletal muscle of Syt VII −/− mice with specific antibodies. Frozen sections of quadriceps muscle of 8-wk-old male WT or KO mice were incubated with biotinylated mAbs to CD3 (T cells), CD11b (macrophages and NK cells), or Ly6G (neutrophils and eosinophils), followed by streptavidin/peroxidase-conjugated secondary antibodies. The first two panels (stained for CD3 and CD11b, respectively) are serial sections, indicating that the same muscle fibers are simultaneously surrounded by T cells and macrophages.

mice of >19 wk old (Fig. 5 C). And, importantly, a strong antinuclear antibody response was detected in the serum of Syt VII–deficient mice at 19 and 44 wk old, but not in younger, 8-wk-old animals (Fig. 5 D). Thus, our findings demonstrate that Syt VII–deficient mice develop a pathology strongly resembling the human autoimmune syndromes polymyositis/dermatomyositis, which are characterized by muscle weakness, focal inflammatory infiltrates, and production of autoimmune antibodies (Casciola-Rosen et al., 2001; Mastaglia et al., 2003).

Conditions leading to autoimmunity are still poorly understood. It is known that self-reactive T cells can be deleted or suppressed in the periphery after the uptake and presentation of self-antigens by antigen presenting cells (Green and Flavell, 1999; Mellman and Steinman, 2001). However, most of the evidence available points to apoptotic cells generated during tissue turnover as the most common source of self-antigens acquired by antigen presenting cells. This steady-state antigen presentation process is thought to lead to tolerance when occurring in the absence of an inflammatory stimulus (Green and Flavell, 1999; Mellman and Steinman, 2001; Steinman and Nussenzweig, 2002). The autoimmune response associated with defective membrane repair in Syt VII–deficient mice suggests that tolerance to antigens released from wounded cells may not be so readily achieved. Such release of intracellular contents mimics necrosis, a process that is proinflammatory and can lead to autoimmunity (Gallucci et al., 1999; Li et al., 2001). In this context, it is significant that the pathology observed in the Syt VII mutant mice occurs largely in tissues under mechanical stress, the skin and skeletal muscle. A similar pattern is observed in human polymyositis (affecting predominantly skeletal muscle) and dermatomyositis (affecting skeletal muscle and skin), suggesting that mechanical injury may represent an important element in the etiology of these serious tissue-specific autoimmune disorders.

## Materials and methods

### Generation of Syt VII −/− mice

A 129-SV/J genomic library (Stratagene) was screened with the rat *Syt VII* cDNA (Martinez et al., 2000) to obtain two phage-carrying overlapping genomic clones encompassing exons 4–6. The targeting vector replaced a 4.2-kb genomic fragment containing exons 4 and 5 with the loxP-flanked neomycin resistance (*neo*) gene expression cassette. The targeting construct was linearized with NotI and electroporated into W9.5 ES cells. 9 out of 160 G418-resistant clones were tested positive for homologous recombination. Five out of these targeted clones were shown to be normal on karyotype analysis, of which two were injected into C57BL/6 blastocysts and transferred into pseudopregnant foster mothers.

### Cells and antibodies

MEF were prepared from day 13.5 embryos (Tournier et al., 2000). Bone marrow–derived macrophages were prepared by flushing tibia and femur bones with Dulbecco's minimal essential medium (DMEM) (Life Technologies) followed by culture in DMEM 10% FBS, and 30% L629 supernatant containing macrophage stimulating factor for 5 d. Syt VII-specific antibodies were generated by immunizing a rabbit with a recombinant GST-fusion

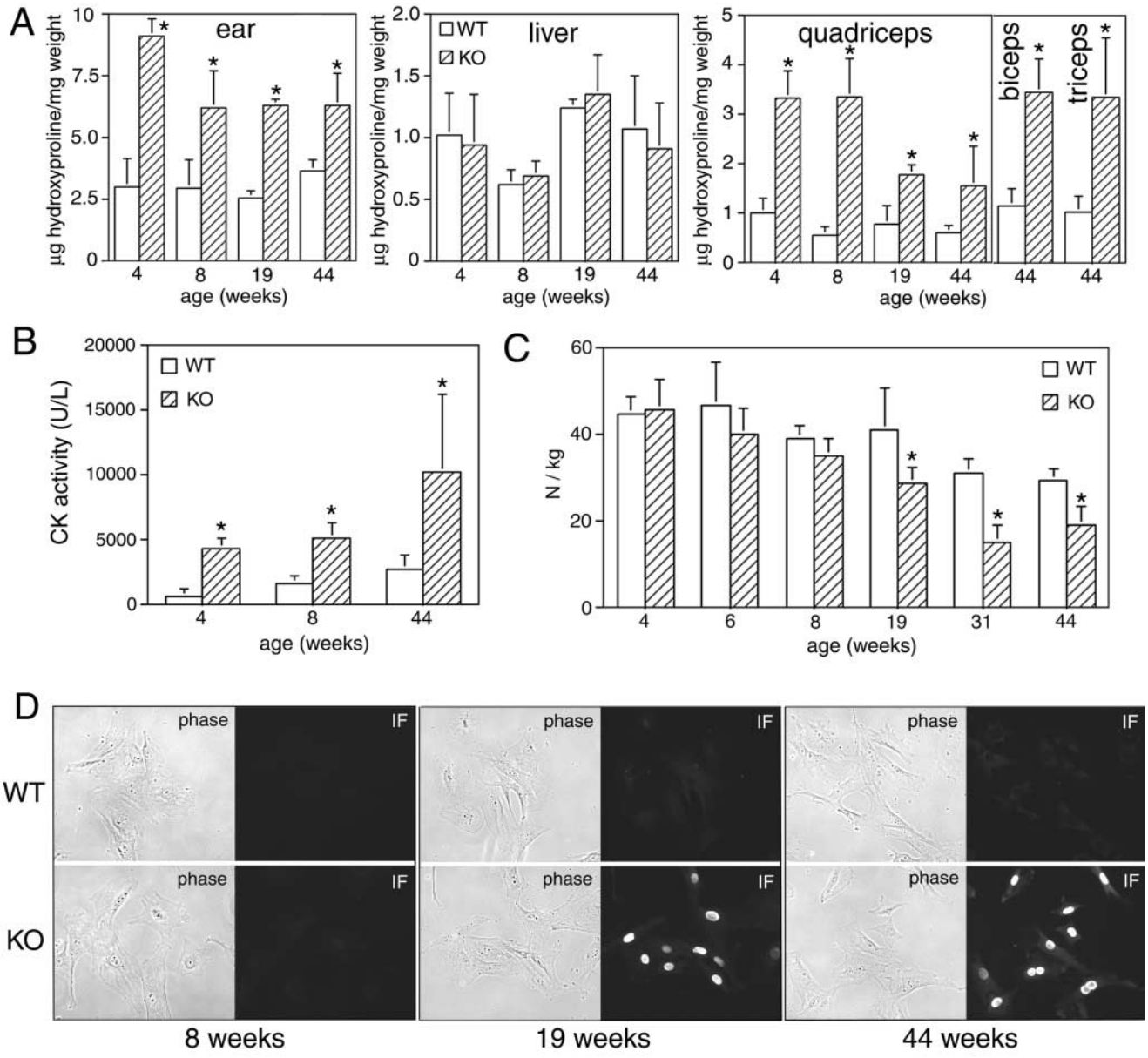


Figure 5. **Myositis symptoms and antinuclear antibody production.** (A) Total collagen content over time in ear, liver, and skeletal muscle from male wild-type (WT) and Syt VII–deficient mice (KO). Tissues were weighed, homogenized, hydrolyzed, and assayed for hydroxyproline content. Each column represents the average ± SD of values obtained from four mice. Asterisk indicates significant differences between the data obtained for KO and WT mice (*t* test, $P < 0.03$). (B) Serum creatine kinase (CK) levels in male WT and KO mice over time. Each column represents the average ± SD of values obtained from four mice. Asterisk indicates significant differences between the data obtained for KO and WT mice (*t* test, $P < 0.05$). (C) Forelimb grip strength over time in male WT and KO mice. Each column represents the average ± SD of measurements made in four to nine mice. Asterisk indicates significant differences between the data obtained for KO and WT mice (*t* test, $P < 0.03$). (D) Generation of antinuclear antibodies in Syt VII −/− mice. Fixed and permeabilized wild-type MEFs were incubated with a 1:100 dilution of serum from 8-, 19-, or 44-wk-old WT or KO mice, followed by FITC-conjugated anti–mouse IgG secondary antibodies.

protein containing amino acids 46–133 of the Syt VII spacer region (Sugita et al., 2001), followed by affinity purification on Affigel (Bio-Rad Laboratories)-immobilized peptide. mAbs specific for CD3 (553239), CD11b (557395), and Ly-6G (553124) were obtained from BD Biosciences. Anti–Lamp-1 mAbs (1D4B) were obtained from the Developmental Studies Hybridoma Bank. Immunofluorescent localization of Lamp-1 and Syt VII was performed on MEFs fixed with 4% PFA in the presence of 0.1% saponin.

### Histological analysis

Killed mice were perfusion fixed with 0.1 M cacodylate buffer, pH 7.4, containing 4% PFA, and 1% glutaraldehyde followed by organ removal, embedding in Epon resin, sectioning, and staining with toluidine blue. Thin sections of Epon-embedded muscle tissue were processed for transmission EM and examined in an electron microscope (Tecnai 12; Philips). H&E or Masson's trichrome staining was performed in paraffin-embedded blocks of tissues previously fixed in PBS containing 4% PFA. Immunocytochemistry was performed on 5-µm transverse cryosections of skeletal muscle using biotinylated mAbs followed by streptavidin-HRP (BD Biosciences) and DAB color development. Sections were examined in a microscope (model Axiovert 135; Carl Zeiss MicroImaging, Inc.) equipped with Metamorph software (Universal Imaging Corp.).

### Hydroxyproline, creatine kinase, and *T. cruzi* invasion assays

Hydroxyproline content in mouse tissues was measured colorimetrically as described previously (Hao et al., 2000). Organs were weighed immediately after removal from killed mice, and the results were expressed as micro-

grams of hydroxyproline per milligrams of tissue. Quantitative, kinetic determination of creatine kinase in serum of control and Syt VII −/− mice was performed as described previously (Bogdanovich et al., 2002). *T. cruzi* invasion of wild-type (WT) and Syt VII–deficient (KO) MEFs was assayed as described previously (Tardieux et al., 1992). At least 200 host cells from randomly chosen microscopic fields were analyzed for each experiment point.

### Grip strength measurement

A grip strength meter (Columbus Instruments) was used to quantify the strength of wild-type and Syt VII −/− mice according to the manufacturer's instructions. Male mice were allowed to grab a triangular ring connected to a tension digital force transducer, and then gently pulled by the tail, away from the bar that measures the maximum tension produced. Three trials were done consecutively on each mouse, with no more than 30 s between each trial. The three values were averaged and correlated with the weight of the animal to generate data expressed as Newton of tension per kilogram of weight of the mouse.

### Wound repair assays using fibroblast-collagen matrices

Suspensions of neutralized Vitrogen 100 collagen (Cohesion Corp.) at 1.5 mg/ml in serum-free DMEM containing $5 \times 10^6$ MEFs/ml were prepared as described previously (Lin et al., 1997; Reddy et al., 2001). The anchored matrices were lifted to initiate cell contraction and wounding by inserting a thin spatula between the collagen matrix and the dish surface. Samples of the supernatant were taken at 2-min intervals, always with replacement of an equal volume of 0.5 ml of fresh media. Background levels of LDH and β-hexosaminidase activity (as determined in Reddy et al., 2001) detected pre-wounding were subtracted from each value. Total β-hexosaminidase and LDH activity was determined in extracts of polymerized matrices treated with 1% Triton X-100 for 30 min.

We thank A. Aderem and M. Reyes-Múgica for valuable discussions; H. Tan for excellent assistance with *T. cruzi* cultures and image processing; and M. Pypaert and the Yale Center for Molecular Imaging for technical assistance.

K. Kobayashi is a recipient of Inflammatory Bowel Disease grants from the Eli and Edythe L. Broad Foundation; R.A. Flavell is an Investigator of the Howard Hughes Medical Institute; and work in F. Gorelick's laboratory is supported by a merit award from the Veterans Administration. This work was supported by a National Research Service Award postdoctoral fellowship to D.R. Liston; a Research Supplements for Underrepresented Minorities award to K. Fowler; by the National Institutes of Health (NIH) and Burroughs Wellcome Scholar awards to N.W. Andrews; and G. Cline, R. LePine, and NIH mouse center grant U24DK-59635.

Submitted: 28 May 2003
Accepted: 7 July 2003

## References

Bai, J., C.A. Earles, J.L. Lewis, and E.R. Chapman. 2000. Membrane-embedded synaptotagmin penetrates cis or trans target membranes and clusters via a novel mechanism. *J. Biol. Chem.* 275:25427–25435.

Bansal, D., K. Miyake, S. Vogel, S. Groh, C.C. Chen, R. Williamson, P.L. McNeil, and K.P. Campbell. 2003. Defective membrane repair in dysferlin-deficient muscular dystrophy. *Nature.* 423:168–172.

Bogdanovich, S., T.O. Krag, E.R. Barton, L.D. Morris, L.A. Whittemore, R.S. Ahima, and T.S. Khurana. 2002. Functional improvement of dystrophic muscle by myostatin blockade. *Nature.* 420:418–421.

Caler, E.V., S. Chakrabarti, K.T. Fowler, S. Rao, and N.W. Andrews. 2001. The exocytosis-regulatory protein Synaptotagmin VII mediates cell invasion by *Trypanosoma cruzi*. *J. Exp. Med.* 193:1097–1104.

Casciola-Rosen, L.A., A.F. Pluta, P.H. Plotz, A.E. Cox, S. Morris, F.M. Wigley, M. Petri, A.C. Gelber, and A. Rosen. 2001. The DNA mismatch repair enzyme PMS1 is a myositis-specific autoantigen. *Arthritis Rheum.* 44:389–396.

Chapman, E.R. 2002. Synaptotagmin: a Ca(2+) sensor that triggers exocytosis? *Nat. Rev. Mol. Cell Biol.* 3:498–508.

Craxton, M., and M. Goedert. 1999. Alternative splicing of synaptotagmins involving transmembrane exon skipping. *FEBS Lett.* 460:417–422.

Fukuda, M., E. Kanno, Y. Ogata, and K. Mikoshiba. 2001a. Mechanism of the SDS-resistant synaptotagmin clustering mediated by the cysteine cluster at the interface between the transmembrane and spacer domains. *J. Biol. Chem.* 276:40319–40325.

Fukuda, M., K. Ibata, and K. Mikoshiba. 2001b. A unique spacer domain of synaptotagmin IV is essential for Golgi localization. *J. Neurochem.* 77:730–740.

Fukuda, M., Y. Ogata, C. Saegusa, E. Kanno, and K. Mikoshiba. 2002. Alternative splicing isoforms of synaptotagmin VII in the mouse, rat and human. *Biochem. J.* 365:173–180.

Gallucci, S., M. Lolkema, and P. Matzinger. 1999. Natural adjuvants: endogenous activators of dendritic cells. *Nat. Med.* 5:1249–1255.

Green, E.A., and R.A. Flavell. 1999. The initiation of autoimmune diabetes. *Curr. Opin. Immunol.* 11:663–669.

Hao, H., D.A. Cohen, C.D. Jennings, J.S. Bryson, and A.M. Kaplan. 2000. Bleomycin-induced pulmonary fibrosis is independent of eosinophils. *J. Leukoc. Biol.* 68:515–521.

Jaiswal, J.K., N.W. Andrews, and S.M. Simon. 2002. Membrane proximal lysosomes are the major vesicles responsible for calcium-dependent exocytosis in nonsecretory cells. *J. Cell Biol.* 159:625–635.

LaMonte, B.H., K.E. Wallace, B.A. Holloway, S.S. Shelly, J. Ascano, M. Tokito, T. Van Winkle, D.S. Howland, and E.L. Holzbaur. 2002. Disruption of dynein/dynactin inhibits axonal transport in motor neurons causing late-onset progressive degeneration. *Neuron.* 34:715–727.

Li, C., B. Ullrich, J.Z. Zhang, R.G.W. Anderson, N. Brose, and T.C. Sudhof. 1995. $Ca^{2+}$-dependent and independent activities of neural and non-neural synaptotagmins. *Nature.* 375:594–599.

Li, M., D.F. Carpio, Y. Zheng, P. Bruzzo, V. Singh, F. Ouaaz, R.M. Medzhitov, and A.A. Beg. 2001. An essential role of the NF-kappa B/Toll-like receptor pathway in induction of inflammatory and tissue-repair gene expression by necrotic cells. *J. Immunol.* 166:7128–7135.

Lin, Y.C., C.H. Ho, and F. Grinnell. 1997. Fibroblasts contracting collagen matrices form transient plasma membrane passages through which the cells take up fluorescein isothiocyanate-dextran and $Ca^{2+}$. *Mol. Biol. Cell.* 8:59–71.

Martinez, I., S. Chakrabarti, T. Hellevik, J. Morehead, K. Fowler, and N.W. Andrews. 2000. Synaptotagmin VII regulates $Ca^{2+}$-dependent exocytosis of lysosomes in fibroblasts. *J. Cell Biol.* 148:1141–1149.

Mastaglia, F.L., M.J. Garlepp, B.A. Phillips, and P.J. Zilko. 2003. Inflammatory myopathies: clinical, diagnostic and therapeutic aspects. *Muscle Nerve.* 27:407–425.

McNeil, P.L., and R.A. Steinhardt. 1997. Loss, restoration, and maintenance of plasma membrane integrity. *J. Cell Biol.* 137:1–4.

Mellman, I., and R.M. Steinman. 2001. Dendritic cells: specialized and regulated antigen processing machines. *Cell.* 106:255–258.

Reddy, A., E. Caler, and N. Andrews. 2001. Plasma membrane repair is mediated by Ca2+-regulated exocytosis of lysosomes. *Cell.* 106:157–169.

Rodriguez, A., P. Webster, J. Ortego, and N.W. Andrews. 1997. Lysosomes behave as $Ca^{2+}$-regulated exocytic vesicles in fibroblasts and epithelial cells. *J. Cell Biol.* 137:93–104.

Steinman, R.M., and M.C. Nussenzweig. 2002. Avoiding horror autotoxicus: the importance of dendritic cells in peripheral T cell tolerance. *Proc. Natl. Acad. Sci. USA.* 99:351–358.

Sugita, S., W. Han, S. Butz, X. Liu, R. Fernandez-Chacon, Y. Lao, and T.C. Sudhof. 2001. Synaptotagmin VII as a plasma membrane Ca(2+) sensor in exocytosis. *Neuron.* 30:459–473.

Tardieux, I., P. Webster, J. Ravesloot, W. Boron, J.A. Lunn, J.E. Heuser, and N.W. Andrews. 1992. Lysosome recruitment and fusion are early events required for trypanosome invasion of mammalian cells. *Cell.* 71:1117–1130.

Tournier, C., P. Hess, D.D. Yang, J. Xu, T.K. Turner, A. Nimnual, D. Bar-Sagi, S.N. Jones, R.A. Flavell, and R.J. Davis. 2000. Requirement of JNK for stress-induced activation of the cytochrome c-mediated death pathway. *Science.* 288:870–874.

Ullrich, B., and T.C. Sudhof. 1995. Differential distributions of novel synaptotagmins: comparison to synapsins. *Neuropharmacology.* 34:1371–1377.

Yoshihara, M., and J.T. Littleton. 2002. Synaptotagmin I functions as a calcium sensor to synchronize neurotransmitter release. *Neuron.* 36:897–908.